Study on Crack Width and Crack Resistance of Eccentrically Tensioned Steel-Reinforced Concrete Members Prestressed by CFRP Tendons

Yu Deng[a], Jinyang Gui[a], Hexin Zhang[b,*], Alberto Taliercio[c], Peng Zhang[a], Simon H F Wong[d], Piti Sukontasukkul[e], Afrasyab Khan[f], Lin Li[g], Yunchao Tang[h], Xingyu Chen[i]

[a] *School of Civil Engineering and Architecture, Guangxi University of Science and Technology, Liuzhou, China, 545006*
[b] *School of Engineering and the Built Environment, Edinburgh Napier University, 10 Colinton Road, Edinburgh, Scotland, UK, EH10 5DT*
[c] *Department of Civil and Environmental Engineering, Politecnico di Milano, Milan, Italy*
[d] *Faculty of Science and Technology, Technological Higher Education Institute of Hong Kong, 20A Tsing Yi Road, Tsing Yi Island, New Territories, Hong Kong*
[e] *Construction and Building Materials Research Center, Department of Civil Engineering, King Mongkut's University of Technology North Bangkok, Thailand*
[f] *Institute of Engineering and Technology, Department of Hydraulics and Hydraulic and Pneumatic Systems, South Ural State University, Lenin Prospect 76, Chelyabinsk, 454080, Russian Federation*
[g] *College of Urban and Rural Construction, Zhongkai University of Agriculture and Engineering, Guangzhou, China*
[h] *Department of Civil and Architectural Engineering, Tennessee State University, Nashville,TN, 37209, USA*
[i] *School of Civil Engineering and Architecture, Guangxi University, Nanning, China, 545006*

Abstract: In recent decades, steel-reinforced concrete (SRC) members under eccentrical tension have been adopted more frequently in modern buildings due to the constraints of more complex structural design/detailing that accompanying contemporary architectural creations. Crack resistance of this type of structures has become a critical design consideration but received insufficient research attention in the past. In this context, the anti-cracking performance of prestressed SRC columns reinforced with CFRP tendons under eccentric tensile loads is investigated experimentally and analytically with the following first-hand experimental validations: 1) prestressed CFRP tendons can well strengthen SRC columns under eccentric tensile load and restrain the crack propagation; 2) an increase in the load eccentricity progressively weakened the influence of prestressing tension level on the cracking load; 3) specimens with the higher prestressed tension level, larger longitudinal reinforcement diameter, and flange thickness exhibited greater crack

* Correspondent author: j.zhang@napier.ac.uk (Hexin Zhang)

resistance capacity. Furthermore, the plane-section assumption was also validated in this study. A test data-enhanced analytical method was proposed for determining the cracking load of PSRC columns.

Keywords: steel-reinforced concrete; crack resistance; eccentric tension; bonded prestressed CFRP tendon; prestressed steel-reinforced concrete

1. Introduction

SRC structures have offered numerous advantages over reinforced concrete (RC) structures, including reduced section size and improved mechanical properties. SRC has become one of the most popular structures for designing high-rise buildings [1-6]. Its development and popularity can be assigned to its higher bearing capacity and better deformation performance. Moreover, it offers a reduced cross-sectional area and increased structure span. Compared with steel structures, the SRC columns have lower construction costs and greater structural stability. Furthermore, the encased steel shape is tightly wrapped by the external concrete, providing it with fireproofing, tensioning, and buckling resistance [7-9]. Numerous studies have addressed SRC columns, mainly focusing on the mechanical properties in terms of compression, bending, shearing, and torsion, while a limited number of studies have considered its tensile properties [10-12].

In recent decades, SRC columns under immense, concrete-unfavourable, tensile loads have become more common in bridge elements, truss transfer layer, and corner columns of low-rise buildings to utilise their prominent mechanical properties, and economical and construction efficiency. Due to the structural complexity of the contemporary architectural innovation, SRC columns may have to undertake adverse eccentrical tension when the structural design/detailing for a centrically tensioned member became unworkable. However, lots of large-scale cracks may form in the concrete areas due to its weakness in tension during their normal service life, which needs to be carefully addressed.

Itou et al. studied earthquake damage in southern Hyogo, Japan, focusing on the axial and eccentric tension of embedded and non-embedded column feet. The findings showed that the non-embedded column footings which used steel-reinforced concrete were destroyed by bending or shearing in tension [13, 14]. Fu et al. experimentally assessed SRC eccentric columns through static tests and nonlinear finite element analysis, resulting in revised recommendations for the bearing capacity formula [15, 16]. Under medium and rare earthquakes, the stress state of eccentric compression columns, such as side and corner columns of high-rise buildings, was likely to transform due to overturning moments, which converted them from axial or eccentric compression to axial or eccentric tension. Eventually, this phenomenon can easily result in rapid destruction.

Furthermore, some adverse effects from the use of SRC structures have been gradually revealed. On the one hand, under the direct tensile load, it is difficult for SRC columns to effectively control and predict the cracking load. Moreover, once the cracks start to develop, cracked concrete quickly exits work and does not involve in the stresses. This results in the rapidly increasing strain at the cracks of the steel bar, leading to large-scale tensile cracks making corrosion and rust unavoidable, thus reducing the structural strength and service life [17]. Prestressing technology, primarily, through the post-tensioning method is one of the popular options to enhance the crack resistance of SRC structures. Prestressing treatment can also prevent corrosion and destruction of the steel upon its exposure to humidity or corrosive environments [18-20]. Scholars have carried out numerous studies on prestressed SRC structures [21, 22].

Fibre-reinforced polymer (FRP) composites have been shown to inhibit crack generation and development, structural reinforcement, and material corrosion resistance [23-28]. To promote the application of SRC structures in China, a prestressed steel reinforced concrete (PSRC) structure with CFRP prestressed tendons was proposed by the authors as an alternative to the SRC columns (Fig. 1). The mechanical behaviour of PSRC columns with steel stranded wire has been assessed over the last few years [29, 30].

Despite the numerous studies in this field, few experimental studies have addressed PSRC columns under eccentric tensile loads, and they were not covered in relevant codes and technical literature. To the best of the authors' knowledge, this study is the first one applying CFRP tendons to PSRC columns under eccentric tensile load. Additionally, the eccentric tensile load was achieved through a loading device with independent intellectual property rights. A total of 11 SRC columns, with a 200×200 mm^2 cross-section and height of 1200 mm, were tested under eccentric tensile loads. The test variables were the load eccentricity, prestressing tension level, longitudinal reinforcement diameter, and steel flange thickness. Then, the distribution of initial cracks in the normal service stage, vertical load maximum versus crack width curves, and the cracking load was systematically examined. Moreover, the design, production, and maintenance of these specimens were carried out simultaneously to avoid the influence of other adverse factors, and ensure that specimens with the same parameters and single variables are comparable. A calculation method was proposed for determining the cracking load through the crack distribution of PSRC columns under a combination of tensile and bending loads. Essentially, this study is aimed at:

a) Study the strength and structural behaviour of the PSRC columns under the eccentric tensile load during the normal operational stage.

b) Evaluate the contribution of prestressed CFRP tendons to crack suppression in PSRC eccentric tensile columns and the influence of four design parameters on the cracking load and maximum crack width, based on the analysis of the prestressed tension level, load eccentricity, longitudinal reinforcement diameter, and steel flange thickness.

c) Establish an analytical model for the calculation of cracking load to predict structural cracking.

d) Analytically assess the effect of prestressed tension level, steel reinforcement diameter, flange thickness, and load eccentricity.

2. Experimental program

2.1 Design of specimens

In this study, 11 SRC columns were prepared and tested under eccentric tensile load. Eight PSRC columns were reinforced with prestressed CFRP tendons, while the remaining three SRC columns had no strengthening agent to serve as the contrast specimens. All the specimens had a 200 mm×200 mm cross-section and a height of 1200 mm. The design parameters were the prestress tension level of CFRP tendons (λ), the load eccentricity ratio (e/h), the longitudinal reinforcement diameter (d), and the steel flange thickness (t_f). Specifically, prestress tension levels of 40% and 60% were designated, where (λ) is the ratio of the pretension stress applied to the CFRP tendons to its ultimate tensile strength. Load eccentricity ratios (e/h) of 0.1 and 0.4 were considered. Moreover, four longitudinal reinforcements of HRB400 grade steel reinforcements with a diameter (d) of 6 mm or 10 mm were arranged at each corner of the specimens. Meanwhile, two steel flange thicknesses (t_f) of the steel section (6 and 8 mm) were taken into account. Moreover, a 7 mm diameter CFRP tendon was adopted, and the steel section was formed by 150 mm×50 mm×6 mm×6/8 mm steel, of grade Q235 according to the Chinese standards. The total height and width of the steel shape are 50 mm, and the steel flange thickness was 6/8 mm while the web thickness was set at 6 mm. Finally, the stirrups of HPB300 grade steel reinforcements with a diameter of 6 mm (spaced at 100 mm, A6 mm@100 mm) were arranged throughout the height of the specimens.

To prevent the slipping of steel and concrete, a row of high-strength studs was arranged on the upper and lower flanges of the steel [31]. The loading end was specially designed to ensure precise force transfer. As shown in Fig. 2, the loading endplate and

concrete end of the specimen have a transition zone in compliance with the requirements of prestressed anchoring and tensioning. To replicate the real scenario of a member under eccentrical tension in a building, i.e. the eccentrical tension force is distributed by the "rigid" joint to the member under the plane-remains-plane assumption, the longitudinal reinforcement, section steel and stiffeners were welded to the loading- endplates. The eccentric tension force is applied and distributed through the endplates.

Specimens were labelled as APZ, SPZ, and LPZ corresponding to the axial tension specimens with an eccentricity ratio of 0, small eccentric tension specimens with an eccentricity ratio of 0.1, and large eccentric tension specimens with an eccentricity ratio of 0.4, respectively. For prestressed columns, their label contains three numbers representing the longitudinal reinforcement diameter, steel flange thickness, and prestressed tension level. However, the label of the non-prestressed columns only had two numbers, indicating their longitudinal reinforcement diameter and steel flange thickness. The detailed parameters of the specimens are listed in Table 1, while the cross-sectional dimensions and geometric structure are depicted in Fig. 2.

2.2 Design of prestressed elements

The prestressing tendons using the post-tensioning method and the prestress loss was calculated according to the Code for Design of Concrete Structures (GB50010-2010) [32], as follows.

$$\sigma_{pc} = \frac{N_{p\mathrm{II}}}{A_n} \tag{1}$$

$$N_{p\mathrm{II}} = (\sigma_{con} - \sigma_l) A_p \tag{2}$$

$$A_n = A_c + \alpha_E A_s \tag{3}$$

Where σ_c is the normal stress in the concrete generated by the prestressing; $N_{p\text{II}}$ is the total pretension in prestressing reinforcement after the complete prestress loss; and σ_{con} is the tension control stress (MPa, $\leq 0.75 f_{ptk}$); σ_l represents a prestress loss value (MPa); A_n is the net cross-sectional area; A_p and A_c are the areas of the prestressing CFRP tendon and the concrete (mm^2), respectively; A_s stands for the area of the steel(mm^2); α_E is the converted modulus of elasticity.

After 28 days of pouring and curing, the specimens underwent the pretension process, using the post-tensioning method through self-designed equipment, as shown in Fig.3. Fig. 3(a) provides a detailed view of the setup clearly, illustrating the components of the device while Fig. 3(b) shows an image of the setup.

The anchor design was employed to decrease the prestress loss and ensure no failure of CFRP tendons at the anchored region [27]. The CFRP anchors, with an anchoring rate of 1.0, were supplied by OVM (Guang Xi CO., LTD). Two sets of hexagonal anchors and metal spacers were included in the post-tensioning equipment. One was placed after the reaction plate, called working anchor #1, and the other was located before the concrete end of the specimens, called post-tensioning anchor #2, for tightening and releasing the force after each tensioning level.

The stressing force was generated using the mono strand hydraulic jacks of 3 tons seated on a special tensioning support. Upon operation, the hydraulic jacks indirectly lift the reaction plate to achieve simultaneous tensioning of the extension screw and CFRP tendons. Note that one end of each CFRP tendon was connected to an extension screw via a connecting sleeve, allowing the CFRP tendons to be indirectly tensioned by tensioning the extension screw which transmitted the tension force. Strain gauges were pasted on the surface of the CFRP tendons to measure the tensioning force due to the hydraulic jack. This method offers more accurate stress data as compared with those only using load cells. The

with an initial force of approximately 10% of the total stressing force, F_s, to close the gaps between components and to remove the slack. F_s was then computed from the control stress in the tendons, which was taken as 0.75 f_{pu} for CFRP tendons. In the second step, CFRP tendons were stressed at six load levels (40% and 60% of total stressing force), as shown in Table 2. Load cells and strain gauges were attached to CFRP tendons to monitor and measure the stresses in the tendons during the whole post-tensioning process.

2.3 Material properties

The mechanical properties of the materials are listed in Table 3. CFRP tendons with a diameter of 7 mm were used, which were supplied by OVM (Guang XI CO., LTD) whose mechanical properties were determined by the tensile test. The properties of the ZH-1 grout material were determined by compression tests on six prisms, splitting tensile tests on six cubes, and bending tests on six prisms. The average compressive strength, splitting tensile strength, and flexural strength were 104.1 MPa, 13.9 MPa, and 38.4 MPa, respectively.

Pre-mixed concrete of C40 was used in the test which was supplied from a local concrete manufacturer. The properties of the concrete were determined according to the Chinese standards (GB/T50152-2012) [33]. Twelve concrete test cubes and nine concrete test prisms were simultaneously used and cured along with the test specimens. The test cubes were 150 mm in length, width, and height, while the test prisms were 150 mm in length and width, and 300 mm in height. On the day of testing, the average compressive strength (f_{cu}) and tensile strength (f_c) of the concrete cubes were 27.4 MPa and 2.83 MPa, respectively. Using conventional steel bars as longitudinal and transverse steel reinforcements, the ultimate tensile strengths of the longitudinally deformed reinforcements, C10, C6, and transverse steel deformed reinforcements, C6, were found to

be 699 MPa, 608MPa and 608 MPa, respectively. Shape steel of grade Q235 and loading endplate of grade Q345 were also applied, whose mechanical properties were reported by the manufacturer after testing six coupons steel specimens according to Chinese standards (JGJ138-2016) [34]. Detailed properties of all the materials are presented in Table 3.

2.4 Measurements, test set up, and loading

Fig. 4 illustrates the details of the setup of the self-developed tension-compression conversion frame for applying the eccentric tensile load. This frame consists of an external and internal truss; the top plate of the outer truss and the bottom plate of the inner truss were fitted with hinged supports. Each of the specimen loading endplates was flexibly connected to the hinged supports by high-strength bolts and nuts, to simulate the real force state. Upon applying pressure by a hydraulic compression machine with a capacity of 5,000 kN to the inner truss, the conversion frame will convert the pressure into a tensile load. Pre-loading was applied, up to 5% of the predicted ultimate capacity, to eliminate the gap between the devices. To accurately observe cracks, before and after the occurrence of the first crack, the applied load was stopped and hold at 5 kN and 20 kN intervals, respectively. A smaller interval before cracking was used to range the cracking load more accurately as it is one of the key parameters in this study. A larger interval was adopted after cracking to minimise the impact of the temporary holds to the overall loading and to reduce the total testing time. And all the specimens were progressively tested under monotonic loads up to yield.

The layout of the linear variable displacement transducers (LVDTs) and strain gauges are presented in Fig. 5. During the loading process, five LVDTs (D_1-D_5) were arranged along the height of the specimen to measure the lateral deflections. To monitor the response of the strain, four (T_1-T_4), nine (T_5-T_{13}), and five (T_{14}-T_{18}) strain gauges were attached to the longitudinal reinforcement, steel shape, and concrete surface at the mid-height of the

specimen, respectively. Additionally, four strain gauges (C_1-C_4) were bonded on the CFRP tendons to measure strain responses and stress loss of the CFRP tendons, as depicted in Fig. 5.

It is worth mentioning that vertical load was applied to the specimen by the loading endplate welded to the steel shape and the longitudinal reinforcement. Various eccentricities were achieved by changing the position of hinge support at the loading end of the specimen, as shown in Fig. 4.

3. Test results and analysis

3.1 Test phenomenon

The results of all the specimens are shown in Table 4, where P_u is the peak load.

Initial cracks： For specimens with eccentricity ratios of 0, 0.1, and 0.4, the horizontal tensile cracks occurred in the tension side of the specimens, when the load reached approximately $0.22\,P_u$, $0.25\,P_u$-$0.34\,P_u$, and $0.18\,P_u$-$0.24\,P_u$ respectively. Most of the horizontal tensile cracks occurred within the middle 1/3 of the specimen height, started from the tension side and propagated towards the compression side across the cross-section. The reason that the tensile cracks started at the middle section is due to the combined effect of tension and bending which formed a maximum tension zone at the middle section of the column. The number of initial cracks of all specimens ranged in 1-3 which propagated slowly with increasing the load.

The overall distribution of cracks： Although the horizontal cracks of all the columns developed at a uniform speed with load increment, no diagonal cracks were observed in the middle of the specimen. Compared with non-prestressed columns, the initial cracks of prestressed columns appeared later with significantly lower quantity. The vertical cracks at

the endplate developed rapidly at the yield load, where the crack height ranged from 150 mm to 320 mm.

3.2 Crack analysis

The fundamental objective of this article is to enhance the crack resistance of SRC columns during normal service life through the use of prestressing tendons. As a result, the cracking load and maximum crack width are the central concerns, however, failure modes of the specimens are not discussed here. The crack distribution (right elevation) of all the columns during normal use is shown in Fig. 6. Combined with the test phenomenon, the studies on crack propagation regularity can be obtained as follows:

There is no significant difference in the patterns of tension crack distribution for all the columns with eccentricity ranges from 0.1 to 0.4. The diagonal cracks close to the end of the column, however, show distinguishing differences among them. For five test specimens with an eccentricity of 0.1, the initial cracks appeared on the eccentric and non-eccentric load sides of the specimen. By continuing the load application, most cracks gradually penetrated the entire section of the specimen. This phenomenon is similar to that of the axial tension specimen with no eccentricity. This is because for small eccentric specimens, the distance of eccentricity is much smaller than the section height, so the performance of small eccentric specimens is very little different from the non-eccentric ones. Another more important reason is that the CFRP prestressed tendon counteracts the eccentric load and offset the effect of small eccentricity so that there is no significant difference to the axial tension. Also, the concrete was directly subjected to tensile stress, resulting in random cracks that could easily penetrate throughout the cross-section.

For five large eccentric columns with an eccentricity of 0.4, horizontal cracks developed from the applied eccentric load side to the other side. Most of the cracks did not propagate through the entire section and crack height was close to the cross-section height of the specimen. Owing to the large eccentricity, the neutral axis of the cross-section

appeared as the load progressed, and the concrete near the applied eccentric load side was subjected to tension, while the other side experienced compression. Cracks are likely to appear in the tension zone due to the lower tensile strength of concrete.

Based on Fig. 6, as the prestress tension level increased from 0% to 40% and then to 60%, the number of cracks and reduced. A significant decline can be observed in the number of cracks upon raising the prestress tension level from 40% to 60%. As the diameter of the longitudinal reinforcements ranged from 6 mm to 10 mm, The number and spacing of cracks remain essentially unchanged, but there is some reduction in crack width for columns with an eccentricity of 0.4. The longitudinal reinforcement diameter showed a more obvious effect on the specimens with a larger eccentricity. However, the flange thickness limitedly influenced crack distribution, number, and spacing on eccentric columns with an eccentricity of 0.4.

3.3 Maximum crack width analysis

Under short-term service load, the maximum crack widths of concrete were carefully measured by the ZW-F160 crack width tester. The relationships between design parameters and the maximum crack width of the midspan zone in the normal limit condition are shown in Fig.7. After comparison, the following conclusions can be drawn.

As shown in Fig. 8(a), with increasing the eccentricity, the maximum crack widths of the specimen with the eccentricity ratio of 0.1 are significantly smaller than the one having the eccentricity ratio of 0.4, indicating the detrimental role of the eccentricity growth in crack control of SRC tensile columns. This phenomenon can be explained by the fact that the tensile load is close to the concrete edge on the eccentric side when the eccentricity ratio reached 0.4, which will greatly weaken the restraint of the stirrups on the concrete.

However, the crack width of SPZ-6-6 is smaller than APZ-6-6, which is related to the heterogeneity and anisotropy of the concrete but is also a good indication of the eccentric specimens with an eccentricity ratio of 0.1 and the axial tension member have similar mechanical properties in terms of the resistance to crack width propagation.

Fig. 7(b) also highlights that maximum crack width can be effectively decreased by prestress level. The level of prestressing is inversely proportional to the rate of crack propagation. This can be attributed to two aspects:1) the prestressing technique can effectively provide the specimens with pre-compression stress to offset the load-generated tensile stress before the cracks arise; 2) CFRP tendons can increase the bending stiffness to delay the crack propagation after its occurrence. Fig. 7(c-d) reveal that the increase in longitudinal reinforcement and flange thickness of the steel section could have a mixed effect on the crack resistance. The level of the eccentricity, the ultimate tensile force achieved in the tests all have an impact on the maximum crack width.

3.4 Cracking load analysis

Table 4 lists the cracking load values of eleven specimens. The following conclusions can be obtained.

The eccentricity ratios of non-prestressed columns (APZ-6-6, SPZ-6-6, and LPZ-6-6) with the same flange thickness and longitudinal reinforcement diameter were 0, 0.1, and 0.4, respectively. By incrementing the eccentricity ratio from 0 to 0.1 and then to 0.4, the cracking load was reduced by 9.3% and 46.6%, respectively, reflecting the significant influence of loading eccentricity on the cracking load of the tensile columns.

The eccentricity ratios of prestressed columns (SPZ-6-6-40, LPZ-6-6-40, SPZ-6-6-60, and LPZ-6-6-60) with the same flange thickness and longitudinal reinforcement diameter were 0.1, 0.4, 0.1, 0.4, respectively. Raising the eccentricity ratio from 0.1 to 0.4 decremented the cracking load by 47.6%, in SPZ-6-6-40 and LPZ-6-6-40, and 42.7% in

SPZ-6-6-60 and LPZ-6-6-60. Therefore, regardless of prestressing, the eccentricity ratio is an important parameter of cracking load.

For similar loading eccentricity, flange thickness, and longitudinal reinforcement diameter, the prestressed tensile levels of the small eccentric columns (SPZ-6-6, SPZ-6-6-40, and SPZ-6-6-60) were 0%, 40%, and 60%, respectively. An increment in the prestressed tension level from 0% to 40% and then to 60% enhanced the cracking load by 64.8% and 22.8%, respectively. Similarly, for large eccentric columns (LPZ-6-6, LPZ-6-6-40, and LPZ-6-6-60) with the same eccentricity, flange thickness, and longitudinal reinforcement diameter, the prestressed tensile levels were 0%, 40%, and 60%, respectively. A rise in the prestressed tensile level from 0% to 40% and then to 60% elevated the cracking load by 61.7% and 34.2%, respectively. These findings indicate the decisive role of the prestressed tension level in boosting the cracking load of the specimen.

For prestressed small (SPZ-6-6-40 and SPZ-10-6-40) and large, (LPZ-6-6-40 and LPZ-10-6-40) eccentric columns, the only difference was the longitudinal reinforcement diameter. By increasing the longitudinal reinforcement diameter from 6 to 10 mm, the cracking load was enhanced by 6.6% and 6.9%, respectively. Therefore, the longitudinal reinforcement diameter is also an important factor in the cracking load.

For the prestressed columns of LPZ-6-6-40 and LPZ-6-8-40 and SPZ-6-6-40 and SPZ-6-8-40, the flange thickness is the variable parameter. Upon increasing the flange thickness from 6 to 8 mm, the cracking load was also increased by 3.0% and 0.3%, respectively, suggesting the influence of flange thickness on the cracking load. Its impact is, however, limited compared with the other design parameters.

Comparing prestressed eccentric columns and non-prestressed axial tensile columns (APZ-6-6), the cracking load of prestressed small eccentric columns (SPZ-6-6-40, SPZ-6-6-60, SPZ-10-6-40, and SPZ-6-8-40) showed 49.5%, 83.5%, 59.8%, and 49.5%, enhancement, respectively; the rate of change in prestressed large eccentric columns (LPZ-

6-6-40, LPZ-6-6-60, LPZ-10-6-40, and LPZ-6-8-40) was -21.6%, 5.2%, -16.5% and -18.6%, respectively. Except for LPZ-6-6-60, the crack resistance was less than that of the non-prestressed axial tension member (APZ-6-6). At a lower prestress level, the load eccentricity showed a limited impact on the cracking load, while the cracking load improved faster as the prestress level increased. The main cause of this phenomenon is the crack resistance and strengthening effect of the CFRP tendons, which outperformed the weakening effect of the eccentricity.

In general, the cracking load increases as the eccentricity decreases and the increment in the prestressed tension level, longitudinal reinforcement diameter, and flange thickness. Among these four design parameters, the prestressed tension level and eccentricity showed the most significant influence on the cracking load. The effect of the longitudinal reinforcement diameter was slightly smaller, whereas the flange thickness did not remarkably affect the cracking load. The crack resistance of prestressed small eccentric columns was much higher than that of non-prestressed axial tension columns. Moreover, when the CFRP tendons reached a higher prestressed tension level, the crack resistance of prestressed large eccentric columns also improved to a certain extent compared to non-prestressed axial tension columns. The above discussion shows the remarkable tension properties of CFRP tendons which could improve the capacity to delay the emergence of cracks in eccentric specimens. Furthermore, the crack resistance of some prestressed large eccentric columns was even better than that of non-prestressed axial tensile columns, suggesting the crack-postponing role of prestressing.

4. Cracking load and maximum crack width calculation

It was assumed that the stress curves of the tensile and compressive concrete are triangular just before cracking [35].

4.1 Elastic analysis and calculation of the pressure relief stage

For SRC specimens, the axial and bending deformation occurred during the test. Numerous studies have developed calculation methods for determining sectional capacity [36]. However, the cracking load should be emphatically focused; as the crack resistance is a vital index in evaluating structural performance. Furthermore, crack control is the essential factor to ensure the normal function and durability of the structure. In this paper, the strength of the steel shape and longitudinal reinforcement of all the specimens was far from the yield strength before the initial cracks arise. Therefore, the elastic stress theory can be used to calculate the cracking load of PSRC columns. The following assumptions were considered:

(1) The CFRP tendons, steel shape, and concrete are ideal elastomers. The stress and strain of the CFRP, steel shape and longitudinal reinforcements show a linear relationship, without considering the strengthening period.

(2) In this study, the specimens were designed to have a full shear connection to prevent the premature failure of the shear connectors. Moreover, the CFRP anchorage works well without failure or slip.

(3) The plane-section assumption is satisfied.

4.1.1 Elastic analysis

Considering the above assumptions, the anti-cracking capacity of PSRC columns under eccentric tensile load can be determined according to the elastic modulus ratio of the steel shape, CFRP tendons, and longitudinal reinforcements. All the materials were converted to concrete to simplify the calculation process; the detailed steps are shown in Fig. 8.

$$n_p = \frac{E_p}{E_c};\quad n_a = \frac{E_a}{E_c};\quad n_s = \frac{E_s}{E_c} \tag{4}$$

Where n_p, n_a, n_s are the conversion modulus of the elastic modulus of CFRP tendons, section steel, and longitudinal reinforcement, respectively; E_p, E_c, E_s and E_a denote the elastic modulus of CFRP, concrete, longitudinal reinforcement, and section steel, respectively.

$$A_n = bh + (n_a - 1)A_a + (n_s - 1)(A_s^{'} + A_s) - A_k \tag{5}$$

Where A_n is the net cross-sectional area of converted concrete; A_p, $A_s^{'}$, A_s, A_a, A_k represent the cross-sectional areas of the CFRP tendons, upper and lower longitudinal reinforcements, steel shape, and prestressed tendon apertures, respectively.

$$y_{1n} = \frac{(n_s - 1)[A_s^{'}a_s^{'} + A_s(h - a_s)] - A_k(h - a_p)}{A_n} + \frac{bh^2/2 + (n_a - 1)hA_a/2}{A_n} \tag{6}$$

As shown in Fig. 9, where y_{1n} shows the distance from the cross-sectional centroid to the concrete edge of the CFRP tendons side; a_s and a_p are the distances from the centroid of longitudinal reinforcement and CFRP tendons to the bottom of the cross-section.

$$y_{2n} = y - y_{1n} \tag{7}$$

Where y_{2n} is the distance from the centroid of the section to the edge of the concrete away from the side of the prestressed CFRP reinforcement.

$$I_n = (n_s - 1)[A_s^{'}(y_{1n} - a_s^{'})^2 + A_s(h - y_{1n} - a_s)^2] + (n_a - 1)[I_a + A_a(y_{2n} - h/2)^2] + bh^3/12 +$$

$$bh(y_{1n} - h/2)^2 - A_k(y_{2n} - h + a_p)^2 \tag{8}$$

In which I_n and I_a are the inertia moments of the net section of concrete and section steel, respectively.

4.1.2 Calculation of the decompression stage

In this test, grouting of all the prestressed specimens began when the tensioning work was completed, and the loading test was carried out immediately after fifteen days of prestressing monitoring. It can be assumed that the prestress losses were finished. Based on the actual conditions of the test, the resultant force, N_{pe}, at the joint point can be obtained by:

$$N_{pe} = \sigma_{pe} A_p - \sigma_{l5}(A_s + A_s^{'} + A_a) \tag{9}$$

Where σ_{pe} is the effective prestress, σ_{l5} is the prestress loss value caused by prestress relaxation, shrinkage, and creep of concrete, and A_p denotes the area of CFRP tendons.

In the full-section decompression stage, the pre-stress produces normal stress on the specimen section, thus the normal stress of concrete, $\sigma_{pc}^{'}$, can be expressed as:

$$\sigma_{pc}^{'} = -\frac{N_{pe}}{A_n} \pm \frac{N_{pe} \times e_{pn}}{I_n} y_{ln} \tag{10}$$

Where e_{pn} shows the distance from the centroid of the net section to the applied load point.

For zero normal stress of concrete at the joint point, the CFRP tendon stress, σ_{p0}, can be expressed as:

$$\sigma_{p0} = (\sigma_{con} - \sigma_l) + \alpha_p \sigma_{pc} \tag{11}$$

After decompression, the join forces, N_{p0}, will be:

$$N_{p0} = \sigma_{\mathrm{p0}} \times A_p \tag{12}$$

4.2 Cracking load calculation

With reference to the Code for Design of Composite Structures JGJ138-2016, the theory for calculating the bearing capacity of eccentric tensile columns and the theory of cracking resistance for ordinary columns, the following basic assumptions were made:

(1) When the eccentric load is applied to the exterior of the section, there will be a compressive zone in the cross-section; while the eccentric load is applied to the interior of the section, the whole cross-section of the member will be in tension.

(2) The eccentricity ratio affects the concrete stresses at the edge of the section, which is linearly proportional to the ratio.

(3) The stiffness of different parts in a cross-section will affect the distribution of the stresses following the stress-strain relationship.

Under short-term tensile load, eccentricity is one of the most important factors that determine the crack resistance for PSRC columns. And a load eccentricity ratio coefficient φ is proposed to estimate the adverse effect of eccentricity on cracking.

$$\varphi = \frac{h-2e}{h} = 1-2\left(\frac{e}{h}\right) \tag{13}$$

While the prestressed CFRP tendons are only arranged on the tension zone eccentrically, it can assume that the section stiffness between the two sides of the member axis is different. For the stress-strain relation in the cracked section, the central axis is used as the separation line, and only the eccentricity ratio is considered in the lower part, while the stiffness and the eccentricity are considered in the upper part. The stiffness coefficient k is proposed, and combined with the experimental data, the weakening effect of stiffness is significantly smaller than the eccentricity ratio. In order to ensure safety and simplification of calculation, k can be taken as:

$$k=\varphi \tag{14}$$

When tensile loads are applied within the section of the member($0 \le \varphi \le 1$), this means that the full section of the member is subjected to tension, as shown in Fig.9.

According to Fig.9, the strain of all materials can be obtained at once.

$$\varepsilon_c = 0.5(\frac{1+\varphi}{2}+1)\varepsilon_{cr} \quad (15)$$

$$\varepsilon_c^{'} = 0.5(\frac{1+\varphi}{2}+\varphi)\kappa\varepsilon_{cr} \quad (16)$$

$$\varepsilon_p = [\varphi + \frac{h-a_p}{h}(1-\varphi)]\varepsilon_{cr} \quad (17)$$

$$\varepsilon_{af} = [\varphi + \frac{h-a_{af}}{h}(1-\varphi)]\varepsilon_{cr} \quad (18)$$

$$\varepsilon_{af}^{'} = [\varphi + \frac{a_{af}^{'}(1-\varphi)}{h}]\kappa\varepsilon_{cr} \quad (19)$$

$$\varepsilon_s = [\varphi + \frac{h-a_s}{h}(1-\varphi)]\varepsilon_{cr} \quad (20)$$

$$\varepsilon_s^{'} = [\varphi + \frac{a_s^{'}(1-\varphi)}{h}]\kappa\varepsilon_{cr} \quad (21)$$

The cracking load N_{cr} of the PSRC member can be expressed as follows from the principle superposition:

$$N_{cr} = \frac{E_c}{2}(A_c\varepsilon_c + A_c^{'}\varepsilon_c^{'}) + A_pE_p\varepsilon_p + b_ft_fE_a(\varepsilon_{af}+\varepsilon_{af}^{'}) + \frac{h_f\text{-}2t_f}{2}t_wE_a(\varepsilon_{aw}+\varepsilon_{aw}^{'}) + A_sE_s\varepsilon_s + A_s^{'}E_s\varepsilon_s^{'} \quad (22)$$

In addition, when tensile loads are applied to the outside of the section($\varphi < 0$), it is clear that the tension zone and the compression zone are existing at the same time.

$$N_{cr} = \frac{f_t+\varphi f_c}{2}A_c + b_ft_fE_a(\varepsilon_{af}+\varphi\varepsilon_{af}^{'}) + A_sE_s\varepsilon_s + \frac{1+\varphi}{2}(h_f\text{-}2t_f)t_wE_a\varepsilon_{aw} + \varphi A_s^{'}E_s\varepsilon_s^{'} \quad (23)$$

The experimental value and calculated value of cracking load are listed in Fig.10, numbers 1 to 11 represent APZ-6-6 ~ LPZ-6-8-40 in that order. As indicated, the predicted values are generally in good agreement with the experimental results. The average value of the ratio between calculation and test results is 0.97 and their corresponding standard deviations is 0.11. The test value is slightly smaller than the calculated value which can be

assigned to three main reasons. Firstly, the columns with tensile and bending loads are more susceptible to concrete heterogeneity. Secondly, the connection joints between the member and the hinge support have a lateral displacement space of 5 mm due to the installation error, which may result in torsional interference during the loading process. Thirdly, the upper and lower steel flanges of the member are provided with high-strength studs, which are subjected to large shear forces under tensile loading. Therefore, this would accelerate the formation of internal micro-cracks around the stud.

However, calculation error (μ_1) of cracking load of all the specimens varied from 1% to 17% in Table 5, with an average ratio of 0.97 and a coefficient of variation of 0.11, reflecting the accuracy of the calculation formula. As a result, the established formulas are validated and can be used to evaluate the cracking capacities of PSRC columns in practice.

4.3 The crack width calculation

Code for Design of Concrete Structures (GB50010-2010) [32] and Code for Design of Composite Structures (JGJ 138-2016) [34] provide the method for evaluating the maximum crack width of concrete ($\omega_{\max}$) based on the theory of bonding-slip.

$$\omega_{\max} = \alpha_{cr}\psi\frac{\sigma_{sq}}{E_s}\left(1.9c_s + 0.08\frac{d_{eq}}{\rho_{te}}\right) \tag{24}$$

with

$$\psi = 1.1 - 0.65\frac{f_{tk}}{\rho_{te}\sigma_{sq}} \tag{25}$$

and

$$d_{eq} = \frac{\sum n_i d_i^2}{\sum n_i v_i d_i} = \frac{4(A_s + A_p + \xi A_a)}{\sum n_i v_i d_i} \tag{26}$$

$$\rho_{te} = \frac{A_s + A_p E_p / E_s + \xi A_a E_a / E_s}{A_n} \tag{27}$$

where α_{cr} is force characteristic coefficient; ψ is the unevenness coefficient of tensile stress of longitudinal reinforcement; σ_{sq} is the equivalent stress of longitudinal reinforcement; c_s is the distance from the outer edge of the outside tension longitudinal reinforcement to the bottom edge of tension zone; d_{eq} is the effective diameter of tensile materials; ρ_{te} is the equivalent ratio of longitudinal tensile reinforcement calculated by effective tensile concrete cross-sectional area; f_{tk} is standard values for axial tensile strength of concrete; c_f is crack calculation coefficient, axial tension columns c_f=1.1 , eccentric tension columns c_f=1.0 ; d_i, n_i, υ_i are the i-th longitudinal reinforcement diameter, number and relative bond characteristics in the tensile zone, respectively.

As a proportional coefficient of steel tensile area, the parameter ξ is introduced in this paper to predict the ratio of tensile area steel to the total area of steel, small eccentric tensile columns (e/h=0.1) with ξ=1 and large eccentric tensile columns (e/h=0.4) are calculated as follows.

$$\xi = [1 - (x - a'_{af}) / (h - a'_{af} - a_{af})] \tag{28}$$

where x is the height of the compression zone of the member section

A comparison of calculation and experimental results of maximum crack widths is presented in Fig. 11. It could be found that the calculation results for the modified method relatively agree well with the experimental results. The Experimental and analytical values for the maximum crack width of the specimens are summarized in Table 6. The average value of the ratio between calculation and test results is 0.96 and their corresponding standard deviations is 0.29.

5. Conclusion

An experimental study was conducted to investigate the crack resistance of eccentrically tensioned SRC Members that are prestressed by CFRP Tendons. Eight prestressed specimens and three non-prestressed specimens were fabricated and tested. An test data-enhanced analytical model and a set of design formulas for estimating the crack load and crack resistance were proposed. The main findings can be summarized as follows：

1. Carbon fibre reinforced polymer (CFRP) tendons were successfully used as prestressed tendons for SRC members under eccentric tension. Their performance meets the structural requirements.

2. The crack resistance has a negative correlation with eccentricity but a positive correlation with prestressing tension level, longitudinal reinforcements diameter, and steel flange thickness.

3. The cracking load of the PSRC member was enhanced by the prestress effect. The prestressed members exhibited higher crack resistance that has led to improved structural safety, durability and service life.

4. The analytical model proposed considered three possible positions of the neutral axis and was used to estimate the cracking load and crack width. This analytical calculation shows good agreement with the experimental result.

Acknowledgements

The authors would like to express their special gratitude to the supports from the National Nature Science Foundation of China (51768008), British Council and Ministry of Education, China (UK-China-BRI Countries Education Partnership Initiative), China Postdoctoral Science Foundation Project (2017M613273XB), and Nature Science

Foundation of Guangxi Zhuang Autonomous Region (2019JJA160137) and Liuzhou Scientific Research and Technology Development Plan (2017BC40202), Royal Academy of Engineering-Visiting Professor (VP2021\7\12), and Royal Academy of Engineering-Industrial Fellowship (IF\192023).

References

1. Oehlers, D., D.J. Oehlers, and M.A. Bradford, *Elementary behaviour of composite steel and concrete structural members*. 1999: Elsevier.
2. Jeong, Y., S.H. Kim, and J.H. Ahn, *Partial-interactive behaviour of steel–concrete members under static and fatigue loadings.* Magazine of Concrete Research, 2005. **57**(5): p. 289-300.
3. Zhang, J. and J. Jia, *Experimental study on seismic behavior of composite frame consisting of SRC beams and SRUHSC columns subjected to cyclic loading.* Construction and Building Materials, 2016. **125**: p. 1055-1065.
4. Melbourne, C., *Composite structures of steel and concrete, Volume 1: Beams, slabs, columns, and frames for buildings.* Engineering Structures, 1997. **4**(19): p. 338.
5. Ebadi Jamkhaneh, M., M.A. Kafi, and A. Kheyroddin, *Behavior of partially encased composite members under various load conditions: Experimental and analytical models.* Advances in Structural Engineering, 2019. **22**(1): p. 94-111.
6. Hansapinyo, C., et al., *Residual Strength of Reinforced Concrete Beams under Sequential Small Impact Loads.* Buildings, 2021. **11**(11): p. 518.
7. Linhai Han, K.Z., Qinghua Tan, et al. , *Performance of steel reinforced concrete columns after exposure to fire: Numerical analysis and application. .* Engineering Structures, 2020. **211**: p. 110421.
8. Qingfeng Xu, C.H., Yong C. Wang, et al. , *Experimental and numerical investigations of fire resistance of continuous high strength steel reinforced concrete T-beams. .* Fire Safety Journal, 2015. **78**: p. 142-154.
9. Zihua Zhang, J.L., Lei Zhang, et al. , *Study on the interfacial shear behavior of steel reinforced concrete (SRC) members with stud connectors after fire.* Frontiers of Structural and Civil Engineering, 2014. **8**(2): p. 140-150.
10. Linhai Han, Q.T., Tianyi Song. , *Fire Performance of Steel Reinforced Concrete (SRC) Structures. .* Procedia Engineering, 2013. **62**: p. 46-55
11. Shiang Zhang, Z.Z., Xiaogang He. , *Flexural behavior of SRC columns under axial and bilateral loading.* Applied Mechanics and Materials, 2012. **166-169**: p. 3383-3390.
12. E.L. Tan, B.U., *Experimental study on curved composite beams subjected to combined flexure and torsion.* Journal of Constructional Steel Research, 2009. **65**(8): p. 1855-1863.
13. ITOU Michio, O.S., TANAKA Hidenori, et al. , *Ultimate strength and ductility of bare type column base connection in SRC structures under high axial tension: (part 5) [C] // Summaries of Technical Papers of Annual Meeting Architectural Institute of Japan, 2000. .* Tokyo: Architectural Institute of Japan, 2000: , 2000: p. 1141-1142
14. FUJIWARA Daiei, S.K., ITOU Michio, et al. , *Ultimate strength and ductility of bare type column baseconnection in SRC structures under high axial tension: (part 14) [C] // Summaries of Technical Papers of Annual Meeting Architectural Institute of Japan, 2004.* Tokyo: Architectural Institute of Japan, 2004: , 2004: p. 1219-1220
15. Jianping Fu, Q.C., Chuan Zhang., *Calculation for ultimate flexural capacity of eccentrically tensioned SRC members with embeded I-shaped steel. .* Journal of Building Structures, 2017. **38**(2): p. 90-98
16. Jinshu Tang, W.H., Su Zhang, et al. , *Experimental study of mechanical behaviors of SRC beams under eccentric tension. .* Industrial Construction, 2015. **45**(8): p. 170-174

17. Peng Zhang, M.S., Yu Deng. , *Study on eccentric tension test and bearing capacity of SRC members.* Journal of Shenyang Jianzhu University, 2019. **35**(3): p. 453-461
18. Deng, Y., et al., *Experimental and analytical investigation on flexural behaviour of RC beams strengthened with NSM CFRP prestressed concrete prisms.* Composite Structures, 2021. **257**: p. 113385.
19. Deng, Y., et al., *Experimental study on shear performance of RC beams strengthened with NSM CFRP prestressed concrete prisms.* Engineering Structures, 2021. **235**: p. 112004.
20. Deng, Y., et al., *Experimental and Analytical Studies on Steel-Reinforced Concrete Composite Members with Bonded Prestressed CFRP tendon under Eccentric Tension* Composite Structures, 2021. **Accepted**.
21. Gangfeng Yao, X.X., *Analytical model and evaluation of maximum crack width for unbonded PSRC frame beam under short-term service load. .* The Structural Design of Tall and Special Buildings, 2019. **28**(16): p. 1667.
22. Vu, N.A., A. Castel , and R. Francois *Effect of stress corrosion cracking on stress-strain response of steel wires used in prestressed concrete beams.* Corrosion Science, 2009. **51**(6): p. 1453-1459.
23. M. Baena, A.T., Ll. Torres, et al. , *Experimental study and code predictions of fibre reinforced polymer reinforced concrete (FRP RC) tensile members.* Composite Structures, 2011. **93**(10): p. 2511-2520.
24. P. Selvachandran, S.A., K. L. Muthuramu. , *Modified frosch crack width model for concrete beams prestressed with CFRP bars. .* Polymers and Polymer Composites, 2016. **24**(7): p. 587-596.
25. P. Selvachandran, S.A., K. L. Muthuramu., *Deflection of steel reinforced concrete beam prestressed with CFRP bar.* Archives of Metallurgy & Materials., 2017. **62**(3): p. 1915-1922.
26. Tan D. Le, T.M.P., Hong Hao, et al. , *Performance of precast segmental concrete beams posttensioned with carbon fiber-reinforced polymer (CFRP) tendons. .* Composite Structures, 2018. **208**: p. 56-69.
27. Ashraf Salah-Eldin, H.M.M., Brahim Benmokran, *Structural performance of high-strength-concrete columns reinforced with GFRP bars and ties subjected to eccentric loads.* Engineering Structures, 2019. **185**: p. 286-300.
28. Tang, Y., et al., *Axial compression behavior of recycled-aggregate-concrete-filled GFRP–steel composite tube columns.* Engineering Structures, 2020. **216**: p. 110676.
29. Yu Deng, X.W., Peng Zhang, *Experimental study on eccentric tensile properties of prestressed steel reinforced concrete columns.* Journal of Building Structures, 2019. **40**(5): p. 115-123.
30. Yu Deng, X.W., Peng Zhang, *Experimental study and calculation for crack control of unbonded prestressed steel reinforced concrete members under eccentric tension. .* Industrial construction, 2019. **49**(8): p. 185-189
31. Yong Yang, Y.C., Wensong Zhang, et al. , *Behavior of partially precast steel reinforced concrete columns under eccentric loading.* Engineering Structures, 2019. **197**: p. 109429.
32. *GB50010-2012: Code for Design of Concrete Structures*. 2012, China Academy of Building Research.
33. *GB/T 50152-2012: Standard for test method of concrete structures*. 2012, China Academy of Building Research.
34. *JGJ 138-2016: Code for design of composite structures*. 2016, China Academy of Building Research.
35. Qi Cao, J.Z., Zhimin Wu, et al. , *Flexural behavior of prestressed CFRP reinforced concrete beams by*

two different tensioning methods. . Engineering Structures, 2019. **189**: p. 411-422.

36. Tan D. Le, T.M.P., Hong Hao, et al. , *Flexural behaviour of precast segmental concrete beams internally prestressed with unbonded CFRP tendons under four-point loading.* Engineering Structures, 2018. **168**: p. 371-383.

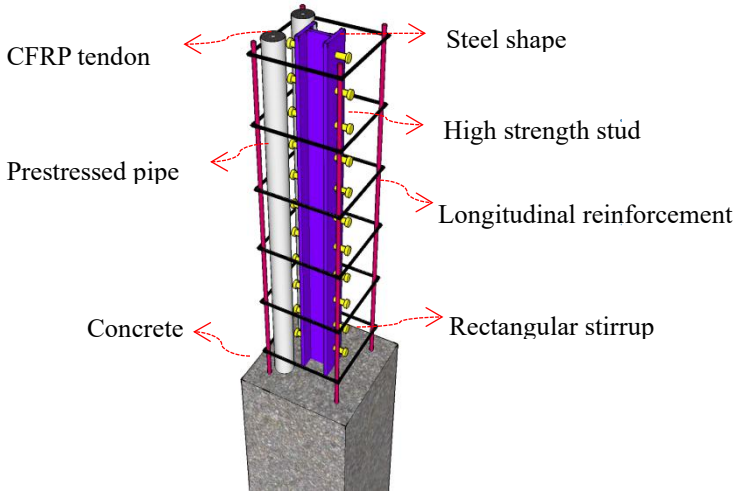

Fig. 1. PSRC members reinforced by prestressed tendons

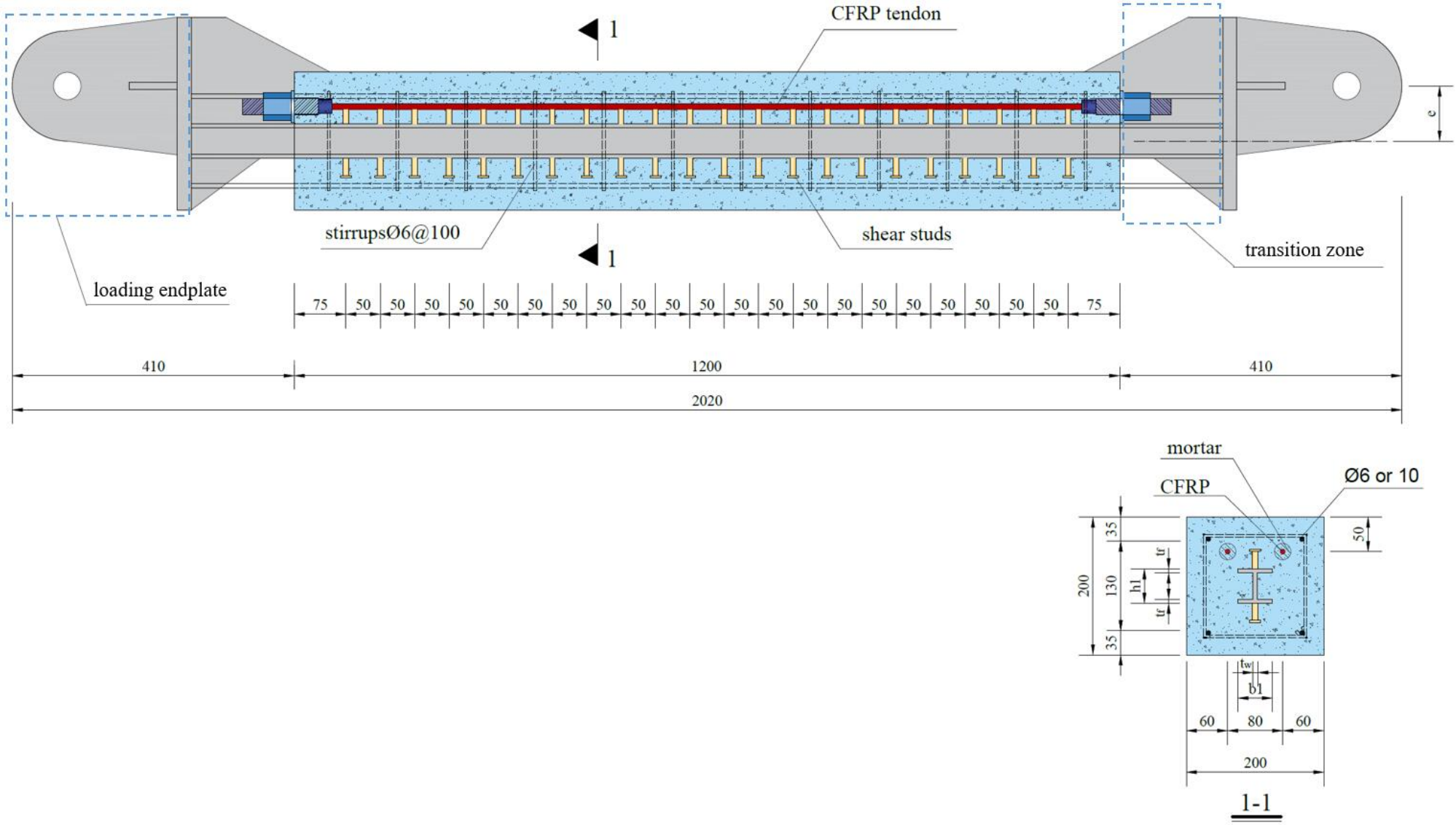

Fig. 2. Detailed design of the specimens (Unit: mm)

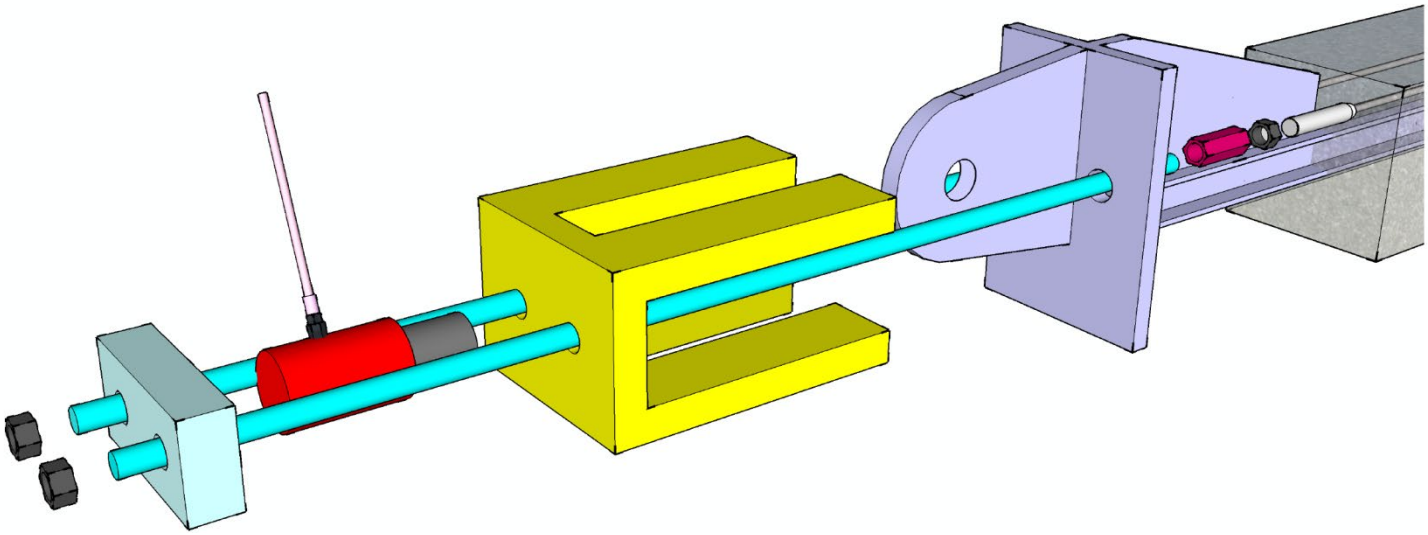

(a) Exploded view of the post-tension hydraulic device

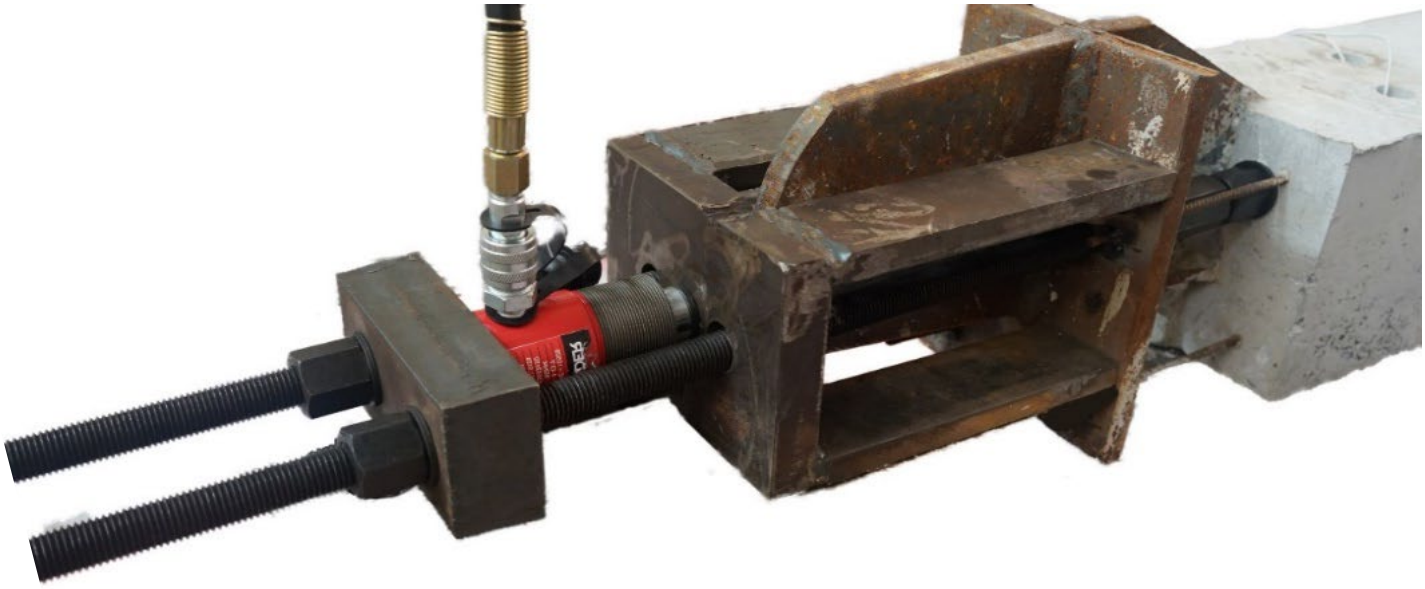

(b) Practicality picture of of the post-tension hydraulic device

Fig. 3. The post-tension hydraulic device

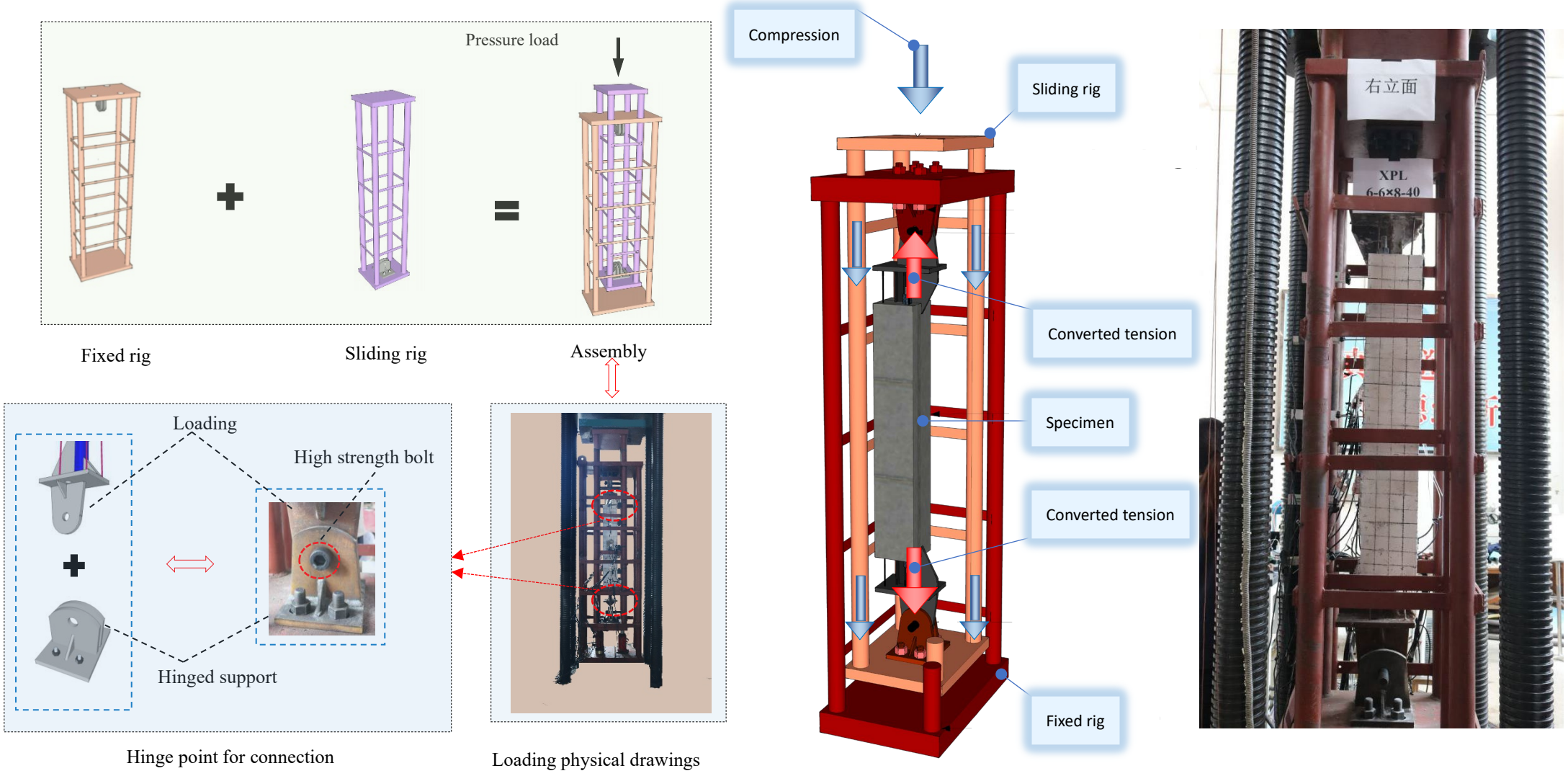

Fig. 4. Details of design and setup of the test rig

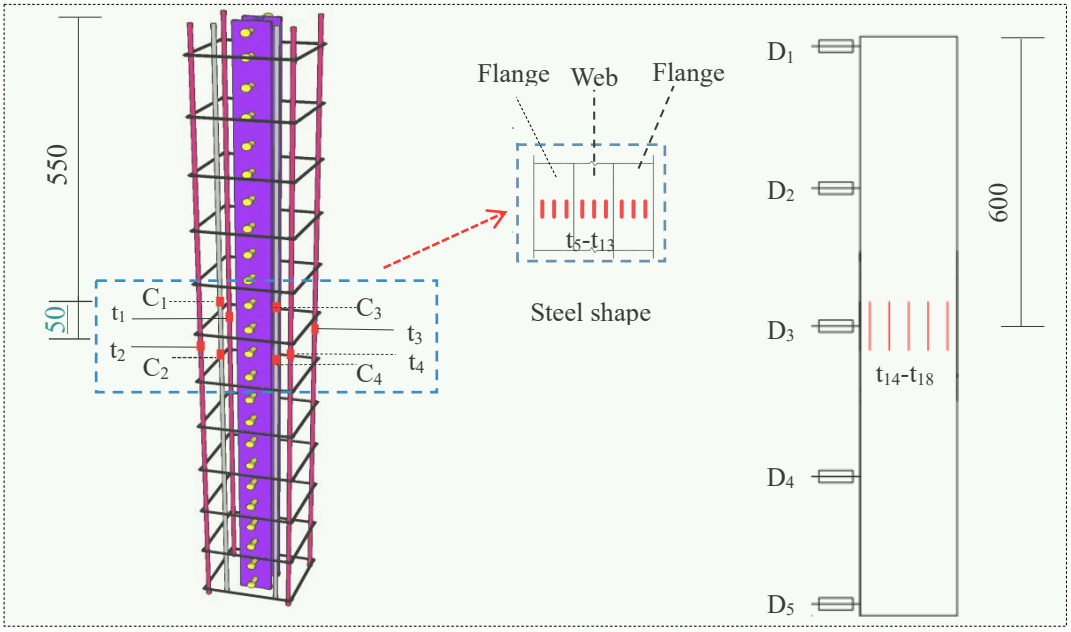

Fig. 5. Layout of measuring points across the specimens (Unit: mm)

(a) APZ-6-6 (b) SPZ-6-6 (c) SPZ-6-6-40 (d) SPZ-6-6-60 (e) SPZ-10-6-40 (f) SPZ-6-8-40

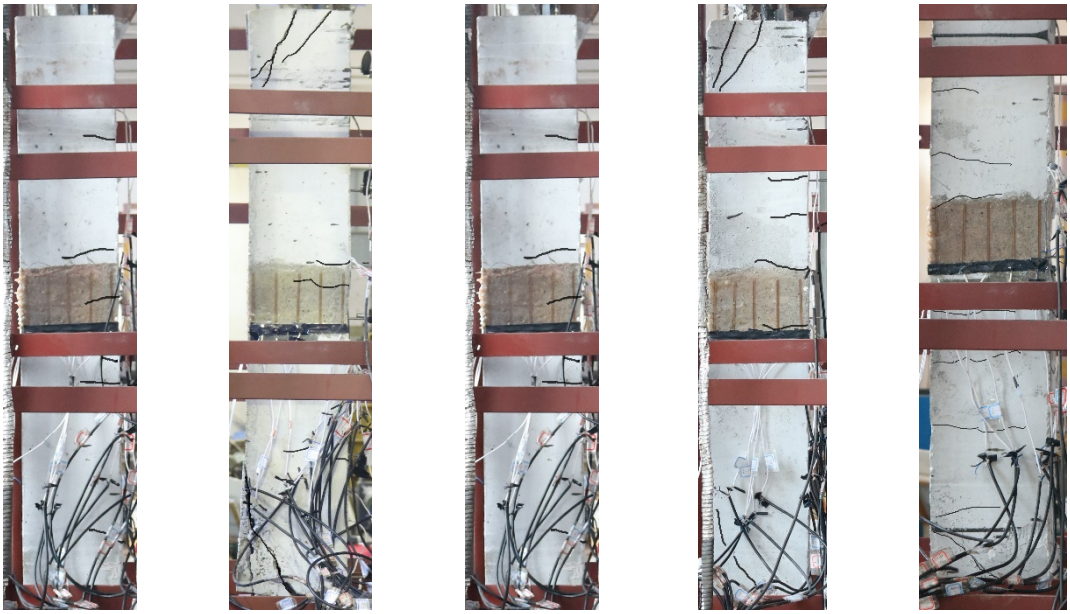

(g) LPZ-6-6 (h) LPZ-6-6-40 (i) LPZ-6-6-60 (j) LPZ-10-6-40 (k) LPZ-6-8-40

Fig. 6. Crack distribution of the ultimate shape of the specimen

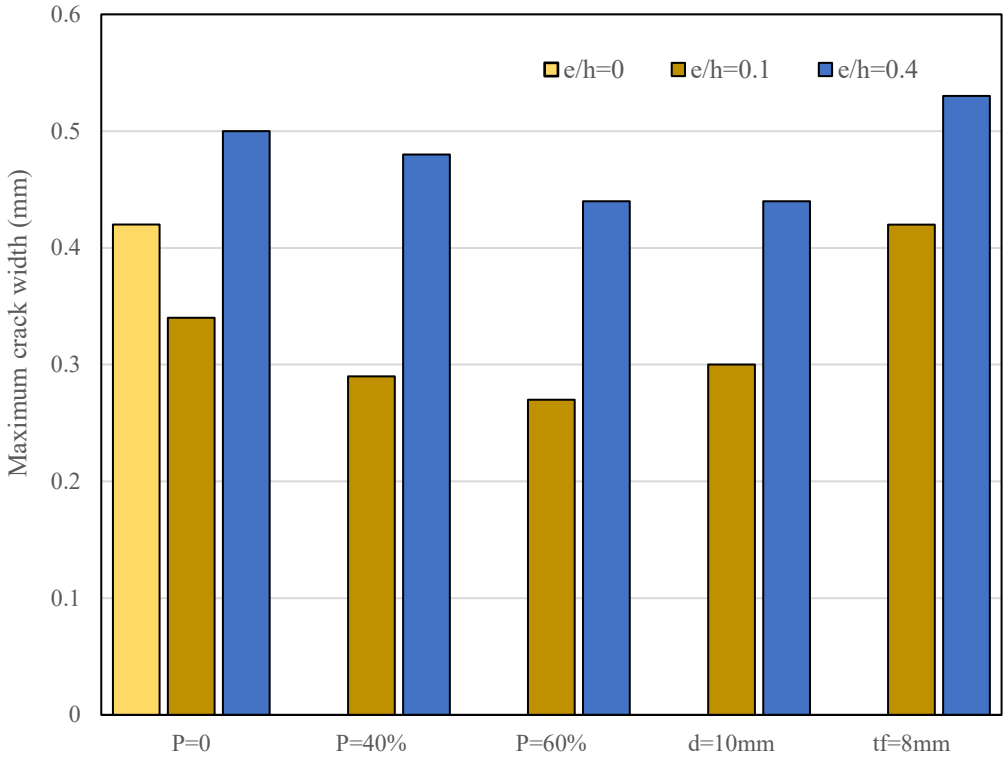

(a) Impact of eccentricity on maximum crack width

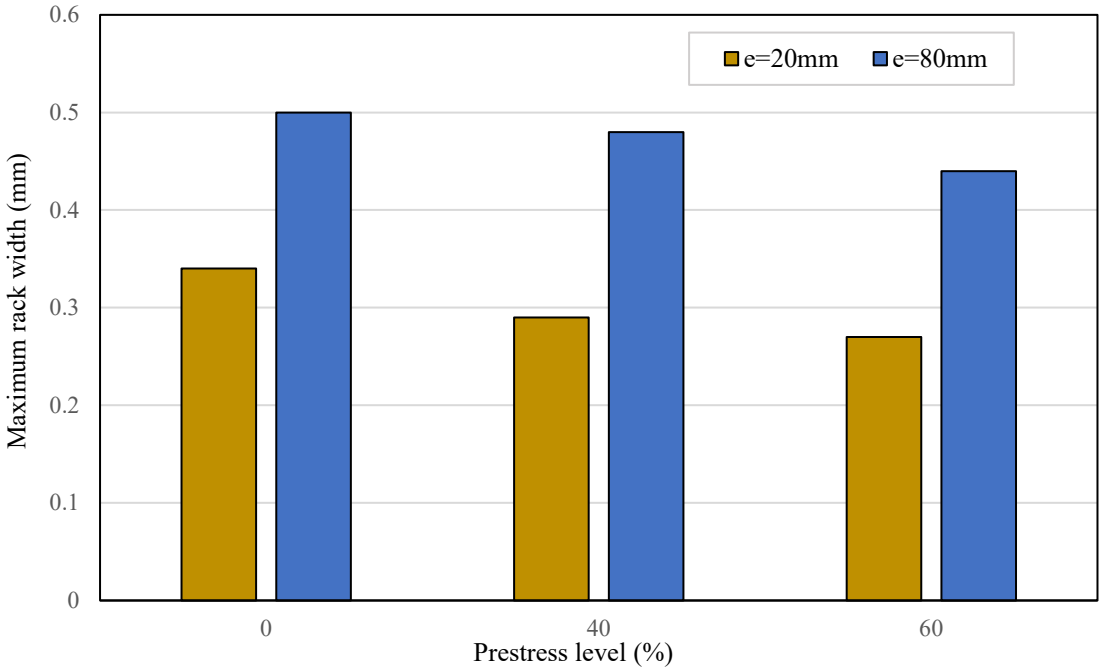

(b) Impact of prestress level on maximum crack width

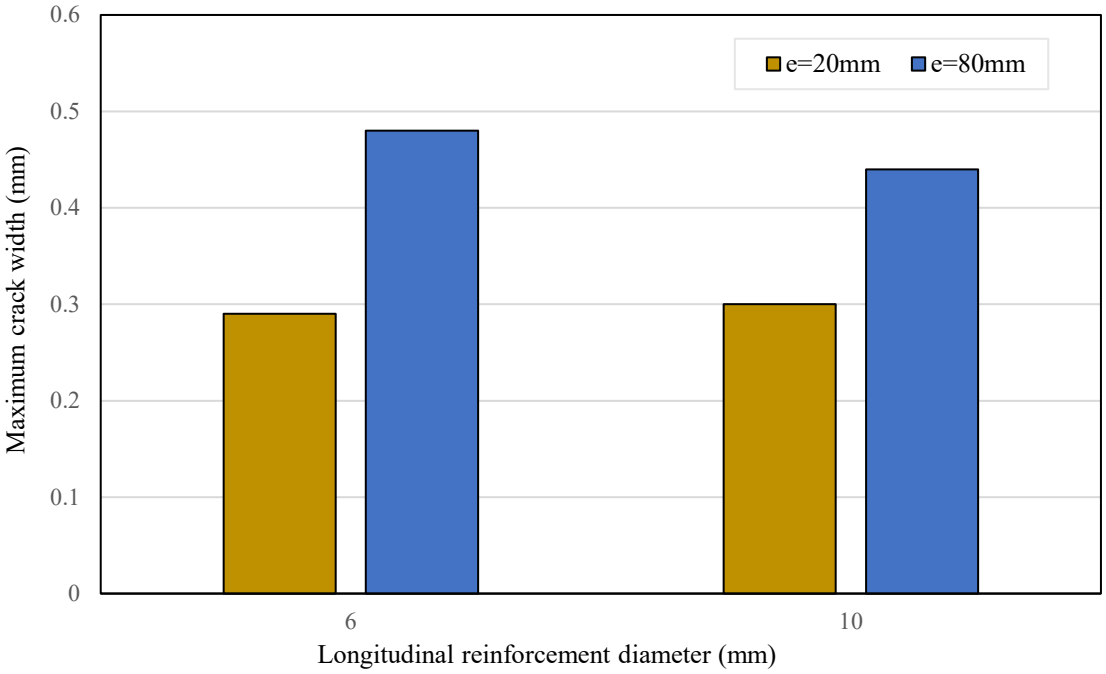

(c) Impact of longitudinal reinforcement diameter on maximum crack width

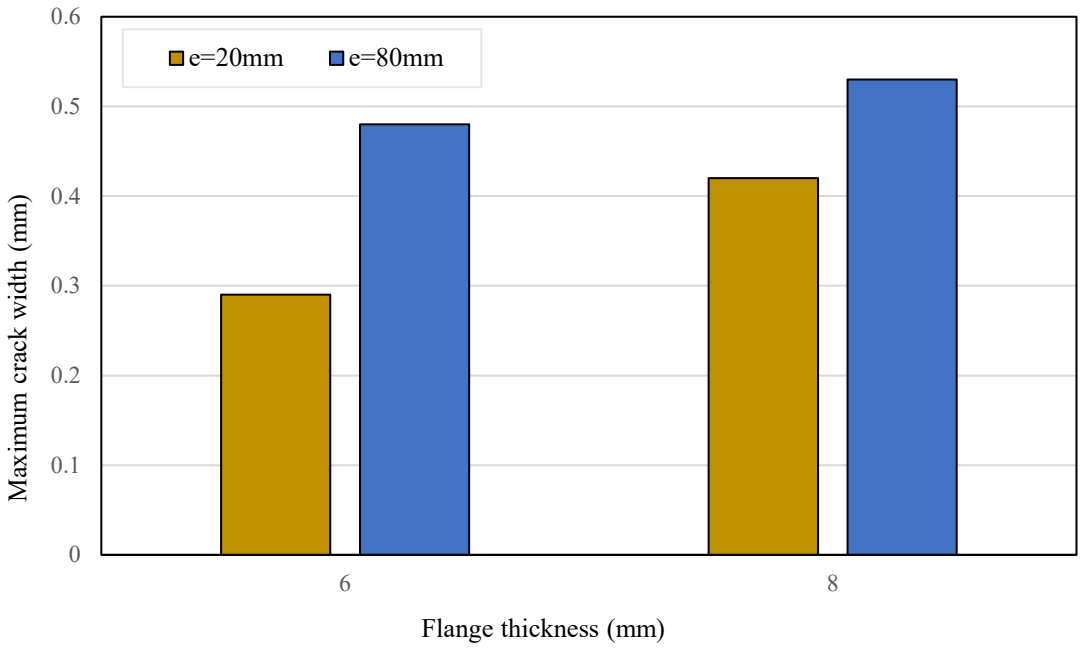

(d) Impact of flange thickness on maximum crack width

Fig. 7. Parameter analysis of maximum crack width

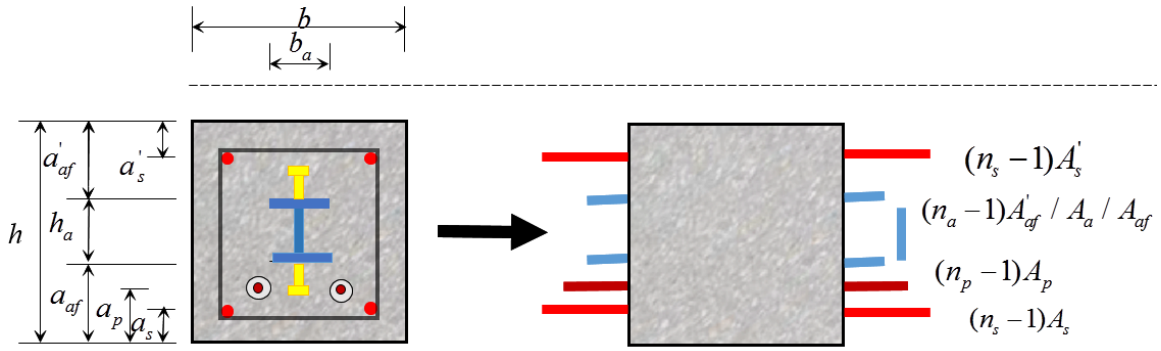

Fig. 8. Conversion section of steel reinforced concrete members with prestressed CFRP tendons

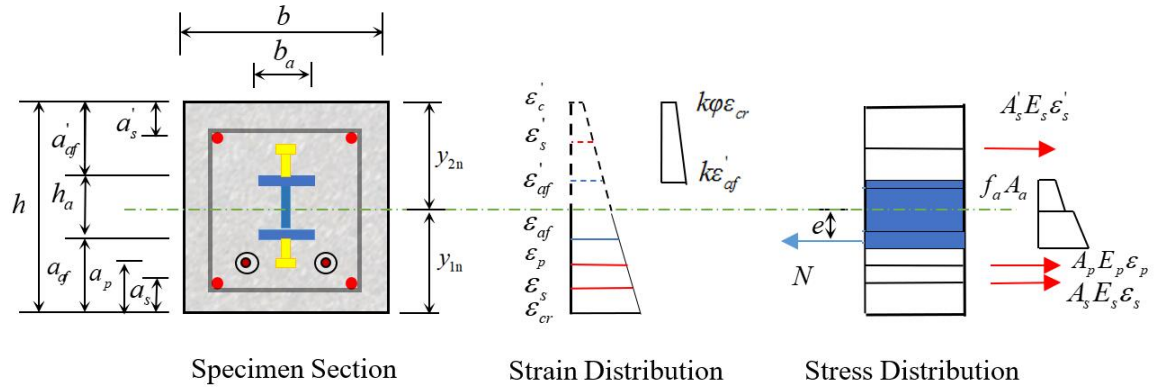

Fig.9. Strain distribution and internal forces across the depth of rectangle section

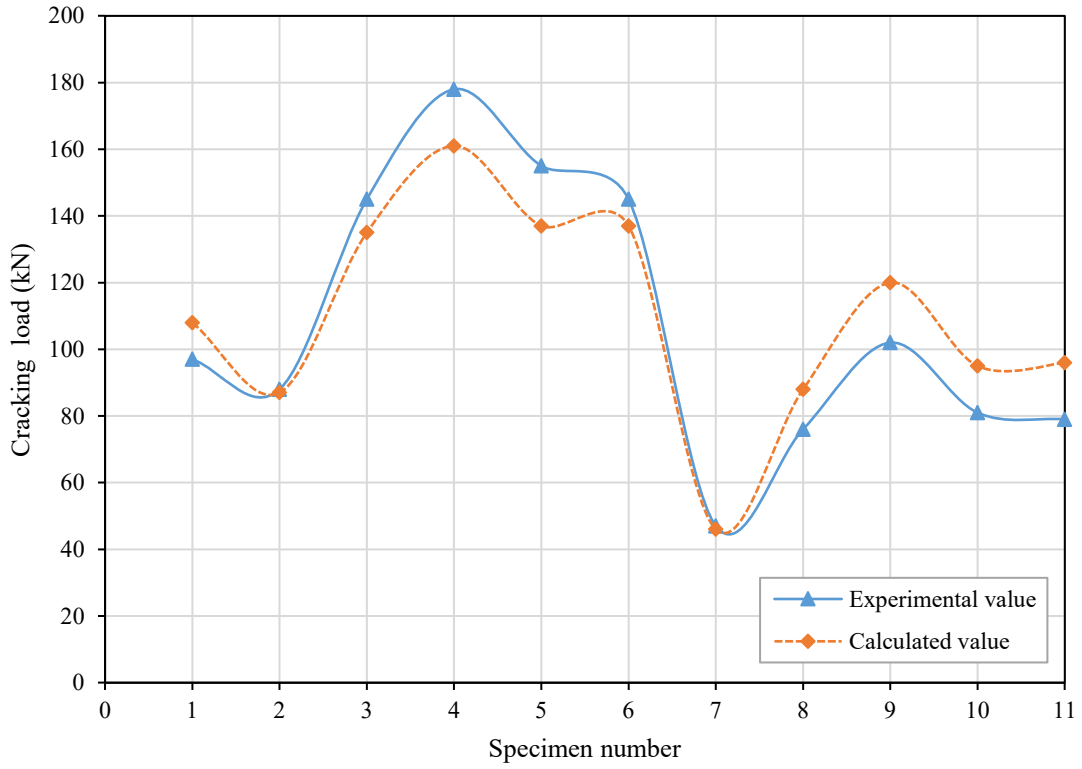

Fig. 10. Comparisons of cracking loading from the experiment and calculated results

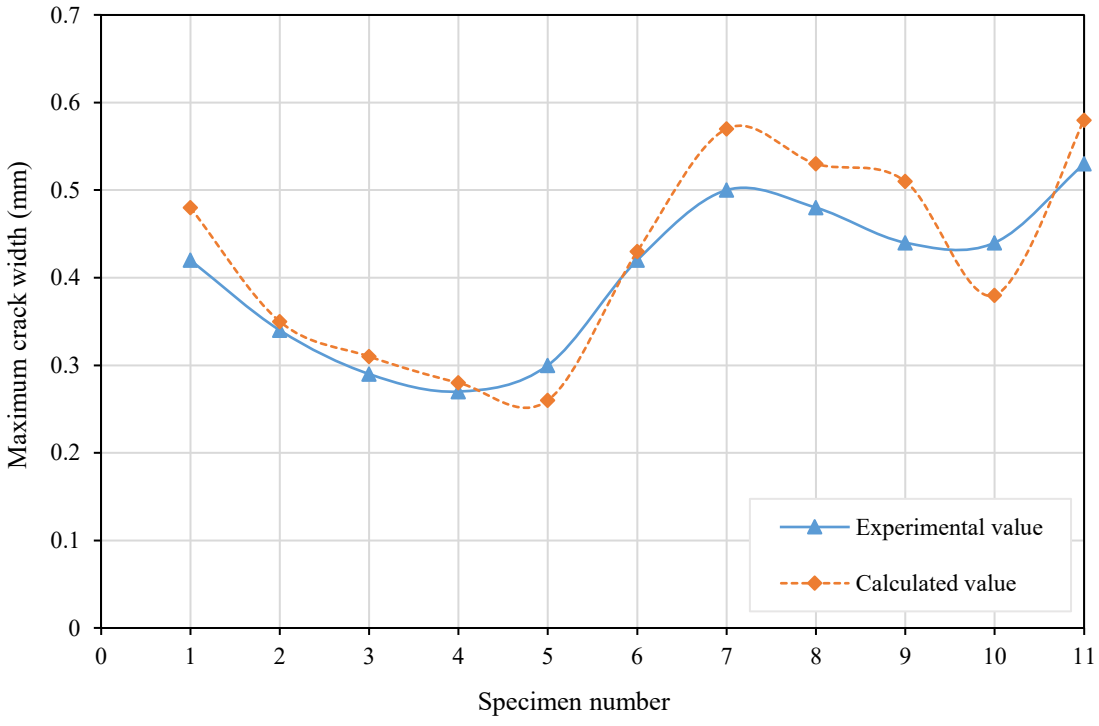

Fig. 11. Comparisons of maximum crack widths from the experiment and calculated results

Table 1

The design parameters of the specimens

Specimen	Eccentricity e (mm)	Eccentricity ratio e/h	Prestressed tension level λ (%)	Longitudinal reinforcement ρ	Flange thickness t_f (mm)
APZ-6-6	0	0	0	4C6	6
SPZ-6-6	20	0.1	0	4C6	6
SPZ-6-6-40	20	0.1	40	4C6	6
SPZ-6-6-60	20	0.1	60	4C6	6
SPZ-10-6-40	20	0.1	40	4C10	6
SPZ-6-8-40	20	0.1	40	4C6	8
LPZ-6-6	80	0.4	0	4C6	6
LPZ-6-6-40	80	0.4	40	4C6	6
LPZ-6-6-60	80	0.4	60	4C6	6
LPZ-10-6-40	80	0.4	40	4C10	6
LPZ-6-8-40	80	0.4	40	4C6	8

Table 2

Control load of CFRP tendons by tension

Tension level	0.2	0.4	0.6	0.8	1.0	1.05
0.4 f_{ptk} [a]	5.9	11.8	17.6	23.5	29.4	30.9
0.6 f_{ptk}	8.8	17.6	26.5	35.3	44.1	46.3

[a] f_{ptk} is the standard value of tensile strength of CFRP tendons.

Table 3

Mechanical property index of materials

Category	Name	Modulus of elasticity E (MPa)	Yield strength f_y (MPa)	Ultimate strength f_u (MPa)	Elongation of material δ (%)
Prestressed tendon	CFRP	1.54×10^5	1624	1910	—
Longitudinal reinforcement	C6	2.00×10^5	495	608	27.5
	C10	2.00×10^5	484	699	25.1
Steel shape	Q235	2.05×10^5	347	481	28.5
Loading plate	Q345	2.05×10^5	458	599	26.3

Table 4

Main test data

Specimen	Total prestress loss σ_l (N/mm^2)	Partial prestress loss σ_{l5} [a] (N/mm^2)	Maximum crack width ω_{max} (mm)	Cracking load N_{cr} (kN)	Variation of N_{cr} (%)	
					λ_1 [b]	λ_2 [c]
APZ-6-6	—	—	0.42	97	—	0
SPZ-6-6	—	—	0.34	88	0	-9.3
SPZ-6-6-40	178.2	46.5	0.29	145	64.8	49.5
SPZ-6-6-60	218.5	69.8	0.27	178	102	83.5
SPZ-10-6-40	164.1	30.8	0.30	155	76.1	59.8
SPZ-6-8-40	175.3	49.3	0.42	145	84.8	49.5
LPZ-6-6	—	—	0.50	47	0	-51.5
LPZ-6-6-40	184	62.4	0.48	76	61.7	-21.6
LPZ-6-6-60	191	64.5	0.44	102	117	5.2
LPZ-10-6-40	166.6	59.9	0.44	81	72.3	-16.5
LPZ-6-8-40	163.2	47.9	0.53	79	68.1	-18.6

[a] σ_{l5} is the prestressed loss caused by prestressed relaxation, concrete shrinkage and creep.

[b] λ_1 is the rate of cracking load variation of prestressed members compared with ordinary eccentric members.

[c] λ_2 is the change rate of cracking load of prestressed and ordinary members compared with axial tension members.

Table 5

Cracking load experimental values and calculation values of the specimens

Specimen	Experimental value $N_{cr,e}$ (kN)	Calculation value $N_{cr,c}$ (kN)	Ratio $N_{cr,e} / N_{cr,c}$	Calculation error μ_1 [a] (%)
APZ-6-6	97	107.5	0.90	10
SPZ-6-6	88	87	1.01	1
SPZ-6-6-40	145	135	1.07	7
SPZ -6-6-60	178	161.3	1.10	10
SPZ -10-6-40	155	137.8	1.12	12
SPZ -6-8-40	145	137.9	1.05	5
LPZ -6-6	47	46.9	1.02	2
LPZ -6-6-40	76	88.2	0.86	14
LPZ -6-6-60	102	120.8	0.84	16
LPZ -10-6-40	81.4	94.8	0.86	14
LPZ -6-8-40	79	95.5	0.83	17

[a] $\mu_1 = \left|1 - N_{cr,e} / N_{cr,c}\right|$

Table 6

Experimental and analytical values for maximum crack width of the specimens

Specimen	Experimental value $\omega_{max,e}$ (mm)	Calculation value $\omega_{max,c}$ (mm)	Ratio $\omega_{max,e} / \omega_{max,c}$	Error μ_2 [a] (%)
APZ-6-6	0.42	0.48	0.88	12
SPZ-6-6	0.34	0.35	0.97	3
SPZ-6-6-40	0.29	0.31	0.94	6
SPZ -6-6-60	0.27	0.28	0.96	4
SPZ -10-6-40	0.30	0.26	1.15	15
SPZ -6-8-40	0.42	0.43	0.98	2
LPZ -6-6	0.50	0.57	0.88	12
LPZ -6-6-40	0.48	0.53	0.91	9
LPZ -6-6-60	0.44	0.51	0.86	14
LPZ -10-6-40	0.44	0.38	1.16	16
LPZ -6-8-40	0.53	0.58	0.91	9

[a] $\mu_2 = \left|1 - \omega_{max,e} / \omega_{max,c}\right|$